

Unbinding transitions of membranes and strings from single and double-well potential

Mesfin Asfaw

Department of Physics and Graduate Institute of Biophysics
National Central University, Jhongli, 32001 Taiwan

April 2, 2008

Abstract

We present a theory of unbinding transitions for membranes that interact via short and long receptor/ligand bonds. The detail of unbinding behavior of the membranes is governed by the binding energies and concentrations of receptors and ligands. We investigate the unbinding behavior of these membranes with Monte Carlo simulations and via a comparison with strings. We derive the scaling laws for strings analytically. The exact analytic results provide scaling estimate for membranes in the vicinity of the critical point.

1 Introduction

Biological membranes consist of a multi-component lipid bilayer with different types of embedded or absorbed macromolecules [1, 2]. They perform a number of general functions in our cells and tissues. For instance, membranes separate cells and cell compartments. They also facilitate the transport of ions and macromolecules into and out of the cells. Some membrane proteins mediate interactions between membranes and participate in cell adhesion [2]. Since membranes play a vital role in biological processes, there are considerable experimental and theoretical interests [3-18].

Membranes undergo both lateral phase separation and unbinding transition. When two membranes interact via short-range attractive potential, the attractive potential forces the membranes to bind. Membranes also exhibit thermally excited shape fluctuations which compete with the molecular force potential. When thermal fluctuations of the membranes are strong enough, membranes undergo a transition from bound state to unbound state at a certain critical temperature T_u and such transition is called unbinding transition.

The study of unbinding transitions of multicomponent membranes has received a significant attention [7,18-22]. In our recent theoretical work [17], we presented a statistical-mechanical model of membranes that interact via two species of receptor/ligand bonds. Tracing out the receptor and ligand degrees of freedom in the partition function leads to an effective double-well potential with effective depths U_1^{eff} and U_2^{eff} . The critical point of lateral phase separation was determined as a function of model parameters. We also predicted the unbinding transition lines for membranes interacting with short and long receptor/ligand bonds by considering membranes that interact via a single-well potential.

In the present work, instead of limiting the study of unbinding transition of membranes to membranes that interact with an effective single-well potential, we consider membranes that interact via an effective double-well potential. This will introduce some additional parameters to the model and, thereby, address a more general problem. We explore the unbinding transition of these membranes via exact analytic results of strings and by comparison with Monte Carlo simulation results.

Some model systems like strings play a crucial role to study the unbinding transition of membranes. Strings are lines governed by tension [20]. Functional renormalization group calculations show that membranes have similar scaling properties as strings in the vicinity of the critical potential depth [23]. Thus, it is worth exploring the scaling behavior of strings. Qualitative similarities between phase diagrams for multi-component membranes and strings have been reported in the work of [24]. In this paper we derive the scaling law for unbinding critical potential depth of strings and suggest a deeper analogy between strings and membranes.

The rest of the paper is organized as follows: In section II we present the unbinding transition of strings that interact with square-well potential. We first give detailed calculation for strings that interact with single-well potential. We then expose the scaling laws of strings that interact with

double-well potential. The strings scaling law is then compared with Monte Carlo simulation results of membranes in section III. Section IV deals with summary and conclusion.

2 String model

Strings are one dimensional lines where their shape fluctuations are governed by a finite tension [20]. We consider here two interacting strings in two dimensional spaces. The conformation of strings can be described by the local separation $l(x)$ perpendicular to the reference line where x measures the distance along the reference line. The strings are, on average, parallel to this line. The effective Hamiltonian of the model

$$H \{l\} = \int_0^L \left[\frac{\sigma}{2} \left(\frac{dl}{dx} \right)^2 + V'(l) \right] dx \quad (1)$$

contains the potential energy $V'(l)$ and σ which denotes the effective tension of the strings.

In the thermodynamic limit the statistical behavior of the model (1) can be explored by transfer matrix method which leads to the Schrödinger-type equation [20, 21, 25]:

$$-\frac{T^2}{2\sigma} \frac{\partial^2 \psi_k}{\partial l^2} + V'(l) \psi_k(l) = E'_k \psi_k(l). \quad (2)$$

Introducing dimensionless variables $E_k = 2E'_k/\sigma$, $z_i = l_i\sigma/T$ and $V(z_i) = 2V'(l_i)/\sigma$, we rewrite Eq. (2) as

$$-\frac{\partial^2 \psi_k}{\partial z^2} + V(z) \psi_k(z) = E_k \psi_k(z). \quad (3)$$

The parameters E_k and ψ_k denote the set of eigenvalues and the wave functions, respectively. The set of eigenvalues $\{E_k\}$ for the above equation is ordered in such a way that $E_0 \leq E_1 \leq E_2 \dots$. The ground-state eigenvalue E_0 gives the free-energy density of the string, $f = E_0$, while the corresponding eigenvector $\psi_0(z)$ determines the probability distribution $P(z)$. The probability distribution $P(z)$ of finding the string at distance z from the reference line is given by

$$P(z) = \frac{|\psi_0(z)|^2}{\int |\psi_0(z)|^2 dz}. \quad (4)$$

The mean and the first moment of the probability distribution is given by $\langle z \rangle = \int z P(z) dz$ and $\langle z^2 \rangle = \int z^2 P(z) dz$, respectively while the string roughness can be written as $\xi_{\perp} = (\langle z^2 \rangle - \langle z \rangle^2)^{1/2}$. On the other hand, in the thermodynamic limit, the parallel correlation length ξ_{\parallel} can be expressed as $\xi_{\parallel} = 1/(E_1 - E_0)$. In the limit $E_1 \rightarrow E_0$, the correlation length ξ_{\parallel} diverges which is the sign of a continuous phase transition taking place in the system.

2.1 Unbinding transition

2.1.1 Single-well potential

From functional renormalization arguments, the scaling behavior of membranes interacting via single-well potential (as shown in Fig. 1) is similar to the scaling behavior of strings interacting via a single-well potential. Strings can be studied with analytical methods. First we explore the behavior of the critical potential depth of strings as a function of the model parameters and finally compare with Monte Carlo results for membranes.

Consider strings interacting via a square-well potential

$$V(z) = \begin{cases} \infty & \text{for } z < 0 \\ -U & \text{for } z_1 < z < z_2 \\ 0 & \text{otherwise} \end{cases} \quad (5)$$

as shown in Fig. 1. The differential Eq. (3) can be easily solved for the square-well potential (5) and the transfer-matrix eigenfunction for the square-well potential (5) has the following form

$$\psi_0(z) = \begin{cases} 0 & \text{for } z < 0 \\ A_1 \exp(kz) - A_1 \exp(-kz) & \text{for } 0 < z < z_1 \\ A_2 \cos(\alpha z) + A_3 \sin(\alpha z) & \text{for } z_1 < z < z_2 \\ A_4 \exp(-kz) & \text{for } z > z_2 \end{cases} \quad (6)$$

Here A_1 , A_2 , A_3 and A_4 are coefficients which are independent of z while the parameters α and k are given by $k = \sqrt{-E_0}$ and $\alpha = \sqrt{E_0 + U}$. One should note that when $E_0 < 0$ the parameter k takes real values and the wave function $\psi_0(z)$ decays as z goes to infinity. This implies that the probability distribution $P(z)$ also decays with z . In this case the average string position $\langle z \rangle$ as well as the string roughness ξ_{\perp} have finite values. When E_0 increases (but remains negative), the value of k gets smaller and the 'tail' of $\psi_0(z)$ lengthens. The probability distribution $P(z)$ becomes broader and hence the

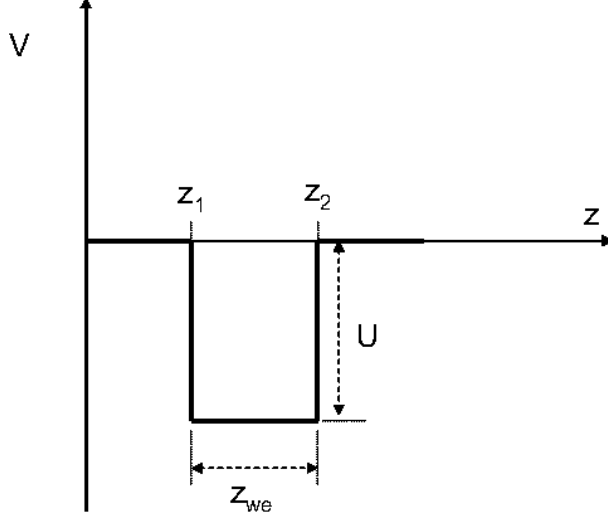


Figure 1: The potential V versus z . The potential has one square well U within the range $z_2 - z_1 = z_{we}$.

average distance $\langle z \rangle$ as well as the string roughness ξ_\perp increase. At $E_0 = 0$ the unbinding transition takes place at which the distribution $P(z)$ becomes flat while $\langle z \rangle$ and ξ_\perp diverge.

The wave function $\psi_0(z)$ and its first derivative $\partial_z \psi_0(z)$ should be continuous at $z = z_1$ and $z = z_2$. These requirements lead to four continuity conditions which finally guide to a transcendental equation. The transcendental equation in principle allows us to determine the free-energy density of the string, $f = E_0$. This transcendental equation is given by

$$2k \exp(2z_1 k) \alpha \eta_1 - (-U + \exp(2z_1 k)(-2k^2 + U)) \eta_2 = 0 \quad (7)$$

where $\eta_1 = \cos(z_{we} \alpha)$ and $\eta_2 = \sin(z_{we} \alpha)$. Here $z_{we} = z_2 - z_1$.

In the limit $E_0 \rightarrow 0$, the critical potential depth U_c can be obtained from Eq. (7) as

$$\cos[z_{we} \sqrt{U_c}] = z_1 \sqrt{U_c} \sin[z_{we} \sqrt{U_c}]. \quad (8)$$

When $z_1 = 0$, the above equation converges to a much simpler expression, $\cos(z_2 \sqrt{U_c}) = 0$, which implies $U_c = \frac{\pi^2}{4z_2^2}$. For $z_1 \neq 0$ equation (8) can be rearranged to

$$z_1 \sqrt{U_c} \tan[z_{we} \sqrt{U_c}] = 1. \quad (9)$$

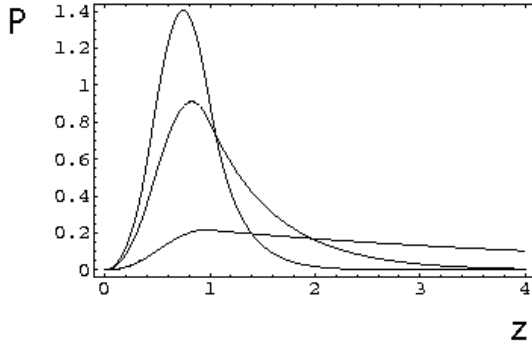


Figure 2: Probability distribution of strings P versus z for fixed $z_{we} = 0.6$ and $z_1 = 0.4$. The potential depths are fixed as $U = 10$, $U = 5$ and $U = 3$ from top to bottom. When the potential depth U decreases the probability distribution becomes broader and flatter.

It is worth to note that for the finite potential width z_{we} , the critical potential depth U_c is different from zero. It means that the unbinding transition takes place at a finite temperature T_c (and therefore it is often called a non-trivial transition). The strings thus are bound in the potential well at low temperature $T < T_c$ (or when $U > U_c$) and unbound from the wall at high temperature $T > T_c$ (when $U < U_c$).

For $U > U_c$, numerically we find how the probability distribution behaves as a function of z as shown in Fig. 2. The figure clearly shows that the strings are strongly localized for the deep potential well. As the potential depth U decreases, the probability distribution P gets flatter.

The numerical solution to Eq. (9) gives us how U_c behaves as function of z_1 and z_{we} as displayed in Fig. 3. Figure 3 shows that U_c decreases monotonously as z_1 and z_{we} increase. This effect can be easily understood. When the distance z_1 increases, the entropic repulsion between strings and the hard wall become weaker. Thus the strings unbind at a lower critical potential depth U_c . When z_1 goes to infinity, strings do not experience the presence of the wall and unbind at $U_c = 0$. On the other hand when z_{we} increases, the entropic loss due to the confinement of strings in the potential well decreases and the strings unbind at shallow critical point U_c .

For fixed $z_{we} = z_2 - z_1$ and in the limit $z_1 \rightarrow \infty$, the effect of the wall is negligible and this corresponds to the case where strings interact with symmetric square well potential which undergoes a delocalization transition

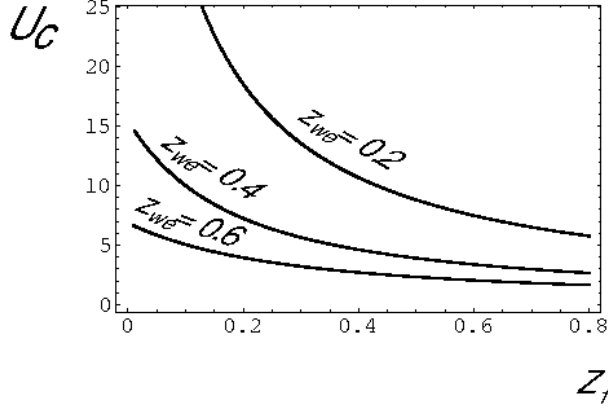


Figure 3: The critical potential depth U_c as a function of the separation field z_1 . The critical potential depth U_c decreases as the parameters z_{we} and z_1 increase. $U_c \rightarrow 0$ in the limit $z_{we} \rightarrow \infty$ or $z_1 \rightarrow \infty$ while $U_c \rightarrow \infty$ in the limit $z_{we} \rightarrow 0$ or $z_1 \rightarrow 0$. Here the potential width is fixed as $z_{we} = 0.2, 0.4$ and 0.6 .

at $U_C = 0$. When $z_1 \rightarrow \infty$, Eq. (7) takes a simple form: $2k\alpha\eta_1 = (-2k^2 + U)\eta_2$. This equation can be rewritten as

$$2\sqrt{-e}\sqrt{e+U} = (2e+u)\tan(z_{we}\sqrt{e+U}). \quad (10)$$

Using trigonometric identity $\tan(z_{we}\sqrt{e+U}) = \frac{2\tan(0.5z_{we}\sqrt{e+U})}{1-(\tan(0.5z_{we}\sqrt{e+U}))^2}$ and applying this trigonometric property, one can rewrite Eq. (10) as

$$2\sqrt{-e}\sqrt{e+U}(\tan(0.5z_{we}\sqrt{e+U}))^2 + (4e+2v)\tan(0.5z_{we}\sqrt{e+U}) - 2\sqrt{-e}\sqrt{e+U} = 0 \quad (11)$$

Solving the quadratic equation (11) for $\tan(0.5z_{we}\sqrt{e+U})$, one gets

$$\sqrt{E_0+U}\tan\left(0.5z_{we}\sqrt{E_0+U}\right) = \sqrt{-E_0}. \quad (12)$$

One can easily notice that when $E_0 = 0$, $U = 0$. This implies the delocalization transition takes place when the potential depth U approaches to zero. In order to explore the thermodynamic behavior of the system in the vicinity of the transition point ($U = 0$), we expand the transcendental equation (12) for a small dimensionless parameter $0 < U \ll 1$. We get a simple expression

for the ground-state eigenvalue E_0 which can be written as $E_0 \approx -\frac{1}{16}U^2 z_{we}^2$. One should note that the free energy density is given by $f = E_0$ and therefore the free-energy density of the string near to the transition point scales as $f \sim -U^2 z_{we}^2$. From this simple scaling law, one can predict the scaling for the contact probability P_C as $P_C \sim -U z_{we}^2$.

The transcendental equation (12) can be rederived for strings interacting via symmetric single-well potential and the method of solving such system is well known [26] and we will not present it explicitly here. Figure 4a shows the probability distribution $P(z)$ for string interacting with symmetric square-well potential of width z_{we} . When the potential well is deep, the strings are strongly localized. As the potential depth U is decreased, the probability distribution $P(z)$ gets flatter and broader. At $U = 0$ the delocalization transition takes place. We also study the behavior of the rescaled probability distribution $P(z/\xi_\perp)$ in the vicinity of the critical point as function of z/ξ_\perp . Figure 4b depicts that after rescaling all the rescaled probability distributions collapse into one scaling function. This reveals that near to the critical point the probability distribution exhibits the scaling form $P(z) = \xi_\perp^{-1} \Omega(z/\xi_\perp)$.

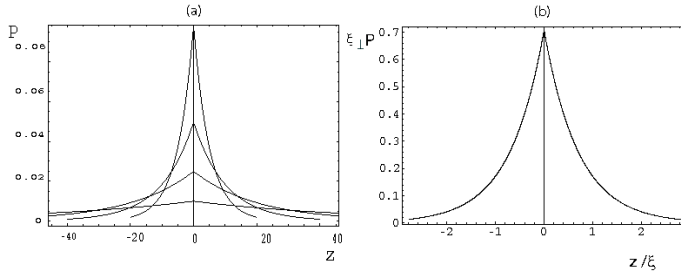


Figure 4: (a) Probability distribution P versus z for fixed values $z_{we} = 0.5$. The potential depth is fixed as $U = 0.4$, $U = 0.2$, $U = 0.1$ and $U = 0.04$ from top to bottom. (b) Rescaled probability distribution $\xi_\perp P$ versus z/ξ_\perp . After rescaling all the curves shown in Fig. 4a collapse onto one scaling function.

2.1.2 Double-well potential

Consider membranes with short and long ligand/receptor bonds. The equilibrium phase behavior of such membranes is governed by an effective double-well potential. Functional renormalization group calculations reveal that membranes have the same scaling behavior as strings in the vicinity of the

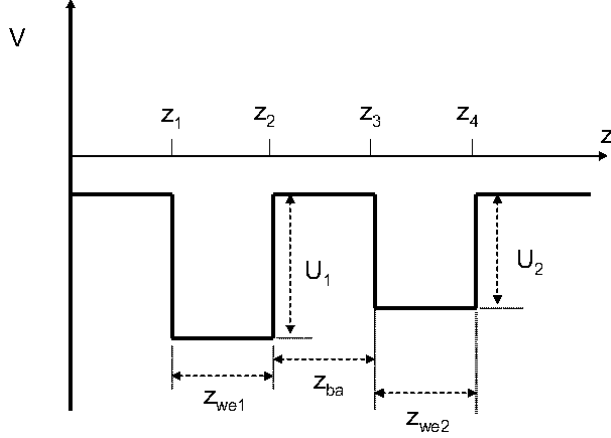


Figure 5: The potential V versus z . The potential has two square wells of U_1 and U_2 within the ranges of z_{we1} and z_{we2} , respectively. The parameter z_{ba} separates the two potential wells.

critical point. The unbinding critical potential depth for strings can be solved exactly using transfer matrix method. First we study the behavior of the critical potential depth of strings that interact with double-well potential as shown in Fig. 5 and latter compare with Monte Carlo results for membranes that interact via double-well potential (see Fig. 5).

Let us now consider strings interacting via double-well potential as shown in Fig. 5. The potential represents the hard wall located at $z = 0$ and two potential wells of rectangular shape. The wave function which satisfies the differential equation (3) has the following form

$$\psi_0(z) = \begin{cases} 0 & \text{for } z < 0 \\ A_1 \exp(kz) - A_1 \exp(-kz) & \text{for } 0 < z < z_1 \\ A_2 \cos(\alpha_1 z) + A_3 \sin(\alpha_1 z) & \text{for } z_1 < z < z_2 \\ A_4 \exp(kz) + A_5 \exp(-kz) & \text{for } z_2 < z < z_3 \\ A_6 \cos(\alpha_2 z) + A_7 \sin(\alpha_2 z) & \text{for } z_3 < z < z_4 \\ A_8 \exp(-kz) & \text{for } z > z_4 \end{cases} \quad (13)$$

The transcendental equation which allows determining the smallest eigenvalue is very complex in this case. Since we are interested in finding the unbinding point, we take the limit $E_0 \rightarrow 0$ and obtain the transcendental

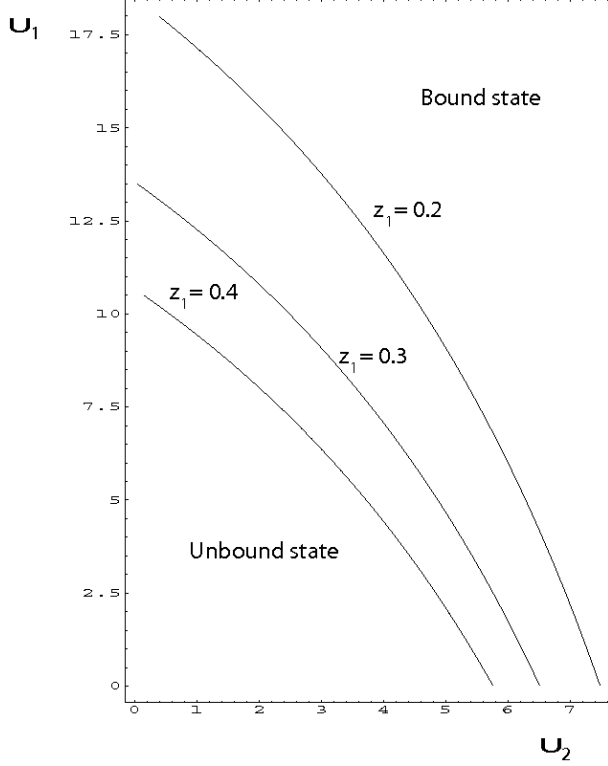


Figure 6: The phase diagram of strings that interact via double-well potential. The strings are unbound for small values of U_1 and U_2 . Here we take $z_{we1} = z_{we2} = 0.2$ and $z_{ba} = 0.2$. As the parameter z_1 increases the phase boundary shifts down.

equation for U_{1c} and U_{2c} as

$$\frac{\sqrt{U_{1c}}(z_1\sqrt{U_{1c}}k_1 + (z_1 + z_{ba})\sqrt{U_{2c}}k_2)}{\sqrt{U_{1c}}k_3 + (z_1z_{ba}U_{1c} - 1)\sqrt{U_{2c}}k_4} = 1 \quad (14)$$

where $k_1 = \cos m_2 \sin m_1$, $k_2 = \cos m_1 \sin m_2$, $k_3 = \cos m_1 \cos m_2$ and $k_4 = \sin m_1 \sin m_2$. We have also introduced : $z_{we1} = z_2 - z_1$, $z_{we2} = z_4 - z_3$, $z_{ba} = z_3 - z_2$, $m_1 = z_{we1}\sqrt{U_{1c}}$ and $m_2 = z_{we2}\sqrt{U_{2c}}$. One should note that in the limit $z_3 \rightarrow \infty$, Eq. (14) converges to Eq. (9) as one expects.

Equation (14) allows us to study how the unbinding critical potential depths U_{1c} and U_{2c} behave as functions of the parameters characterizing the model. Figure 6 shows the phase diagram in U_1 and U_2 parameter space for

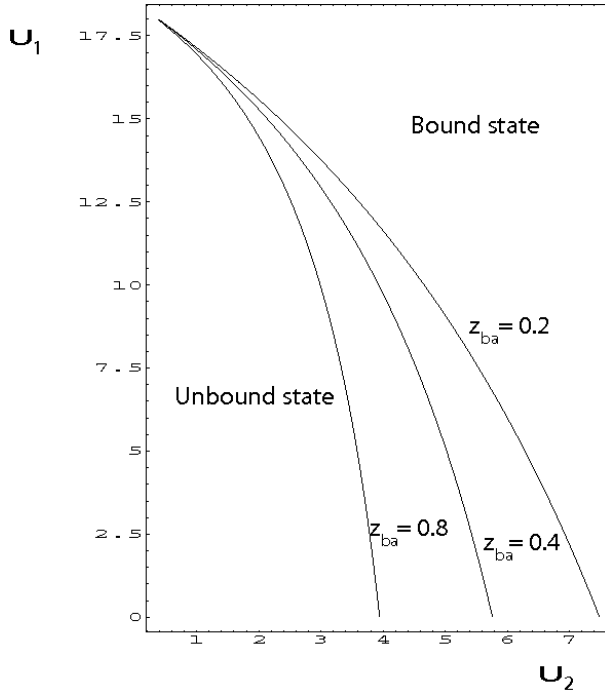


Figure 7: The phase diagram of strings that interact via double-well potential. We take $z_{we1} = z_{we2} = 0.2$ and $z_1 = 0.2$. As the parameter z_{ba} increases the phase boundary shifts to the left.

$z_{ba} = 0.2$ and $z_{we1} = z_{we2} = 0.2$. As demonstrated in the figure, as z_1 increases the phase boundary shifts down. One can note that when z_1 increases, the entropic repulsion of the strings with hard wall decreases. Therefore the strings unbind at lower critical potential depth. In the limit z_1 goes to infinity, the strings do not feel the presence of hard wall. Hence in the limit $z_1 \rightarrow \infty$, $U_{1c} \rightarrow 0$ and $U_{2c} \rightarrow 0$. One should note that even if $z_{we1} = z_{we2}$, the phase diagram 6 is asymmetric due to the fact that strings in the first potential well experience higher entropic repulsion from the hard wall than the strings that are confined in the second potential well. The effect of z_{ba} on the phase diagram is also investigated. Figure 7 depicts the phase diagram in the parameter space U_1 and U_2 for values $z_{we1} = z_{we2} = 0.2$ and $z_1 = 0.2$. As shown in the figure, as the parameter z_{ba} increases the phase boundary shifts to the left. It is important to note that since the values of z_1 , z_{we1} and z_{we2} are fixed, when z_{ba} increases only the position of the second potential well (well-two) shifts to the right. The critical potential depth U_{1c} remains unaffected while z_{ba} increases. On the other hand, when z_{ba} increases, strings confined in the well-two experience a lesser entropic repulsion with the hard wall and due to this the strings unbind at lower critical potential depth U_{2c} .

3 Comparison of membrane and string models

3.1 Unbinding from single-well potential

Consider membranes that interact with receptor/ligand bonds of two different lengths. As presented in the work [17], tracing out the receptor and ligand degrees of freedom in the partition function leads to an effective double-well potential with potential wells of U_1^{eff} and U_2^{eff} . In this section we consider membranes interacting via an effective single-well potential as shown in Fig. 1. We determine the unbinding critical potential depth U_C^{eff} with the Monte Carlo simulations. Within the Monte Carlo simulations, we consider the discretized Hamiltonian [17] and the effective single-well potential as shown in Fig. 1. The separation field z_i of patch i is shifted to another new value $z_i + \xi$. Here ξ denotes a random number between -1 and 1 . We follow the standard Metropolis algorithm [27]. When the change in configuration energy ΔH is negative, a local move is accepted; when ΔH is positive, the local move is accepted with the probability $\exp[-\Delta H]$. In the simulations, membranes

of size $N = 120 \times 120$ patches are considered and to obtain a better statistics, the simulation is performed with up to 10^7 attempted local moves per site i . In the vicinity of the critical point, both the autocorrelation time and correlation length diverge. Thus the simulation is performed for $U^{eff} > U_C^{eff}$. The critical point is obtained by measuring the contact probability $\langle P_b \rangle$ in the simulation. Here $\langle P_b \rangle$ represents the expectation value for the fraction of bound membrane segments in the potential well. One should note that $\langle P_b \rangle$ is independent of the finite size of membranes [17]. The critical point is determined by extrapolating of $\langle P_b \rangle$ as a function of U^{eff} to the critical values $\langle P_b \rangle = 0$.

The plot of U_C^{eff} as a function of z_{we} and z_1 is displayed in the Fig. 8. This result qualitatively agrees with the string result which is shown in Fig. 3. The figure demonstrates that U_C^{eff} decreases monotonously as z_{we} and z_1 increase. When z_1 increases, the steric repulsion of membranes with hard wall decreases. Therefore, membranes unbind at shallow critical potential depth. One should note that for membranes with one types of stickers, integrating out stickers of degree of freedom leads to an effective potential in the partition function. Increasing the separation field z_1 corresponds to the increase in the length of the stickers. The result depicted in Fig. 8 shows that the unbinding transition takes place at lower critical potential depth (at higher temperature) when the length of the stickers increase. The depth of the critical point also depends on the width of the potential z_{we} . The analytic results of string (see Fig. 3) and the numerical results of membranes (See Fig. 8) show that the critical potential depth decreases as z_{we} increases. When z_{we} increases, the entropic loss due to confinement of strings in the potential well decreases and the strings or the membranes unbind at shallow critical point.

Functional renormalization indicates that the critical potential depth of membranes and strings have similar scaling properties [20]. Strings interacting via single-well potentials have scaling properties $\sqrt{\bar{U}_c} z_1 \tan \sqrt{\bar{U}_c} z_{we} = 1$ as discussed in the previous section. Since membranes and strings have similar scaling properties, we postulate the relation

$$\sqrt{U_c^{eff}} z_1 \tan \sqrt{U_c^{eff}} z_{we} = C \quad (15)$$

to hold true for membranes. The constant C can be obtained from data fitting. There is a slight difference between this work and the previous work [17]. In this work we don't consider the approximation $(z_2 - z_1) \sqrt{U_c^{eff}} \ll 1$.

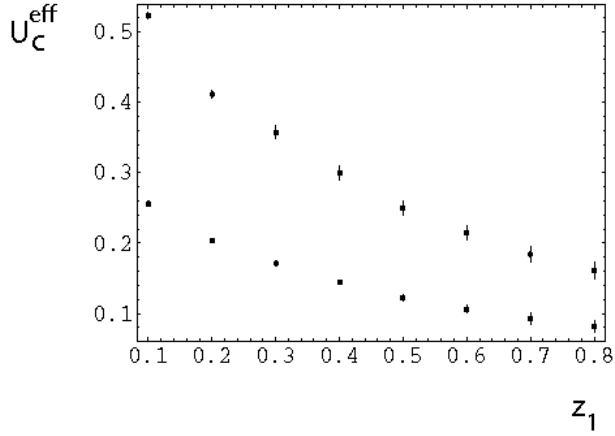


Figure 8: Monte Carlo data for critical potential depth U_C^{eff} of unbinding from the single-well potential as a function of separation field z_1 for $z_{we} = 0.2$ and $z_{we} = 0.4$ from top to bottom. The critical potential depth U_C^{eff} decreases as the parameters z_1 and z_{we} increase.

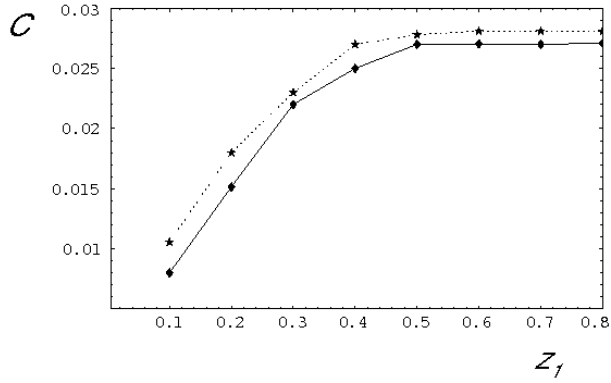


Figure 9: The constant C which represents the scaling law (15) for $z_{we} = 0.4$ and $z_{we} = 0.2$ from top to bottom. The value C is obtained by substituting the Monte Carlo data (see Fig. 8) in Eq. (15). The scaling law is valid for large values of z_1 and z_{we} .

We substitute the corresponding values of U_c^{eff} , z_{we} and z_1 (see Fig. 8) in Eq. 15 and evaluate the constant C . Figure 9 shows how C behaves as a function of z_1 . As indicated in the figure, when z_1 increases C goes to a constant $C = 0.0281 \pm 0.0024$. Here C varies for small values of z_1 since we consider strings in the continuum limit while the membranes here are discretized. In the discrete model, the continuum limit is reached for large values of z_1 and z_{we} .

3.2 Unbinding from double-well potential

Let us now consider membranes that interact via short and long stickers. Tracing out stickers degree of freedom leads to membranes that interact with an effective double-well potential with potential wells of U_1^{eff} and U_2^{eff} [17]. Similar to the previous section, the unbinding critical potential depths U_{1C}^{eff} and U_{2C}^{eff} are determined in the simulation for different values of z_1 , z_{we} and z_{ba} .

Figure 10 reveals the phase diagram in U_1^{eff} and U_2^{eff} parameter spaces for fixed $z_2 - z_1 = z_{we1} = 0.3$, $z_4 - z_3 = z_{we1} = 0.3$ and $z_3 - z_2 = z_{ba} = 0.2$, $z_1 = 0.1, 0.2$ and 0.3 . The figure shows that as the parameter z_1 increases, the phase boundary shifts down. It is important to note that increasing the separation field z_1 corresponds to the increase in the length of short and long stickers. The same figure demonstrates that as the length of short and long stickers increases, the critical potential depths U_{1C}^{eff} and U_{2C}^{eff} decrease. This result qualitatively agrees with the analytical result of string which is shown in Fig. 6.

We also investigate the phase behavior of membranes as a function of z_{ba} for fixed z_1 and z_{we} . Our analysis demonstrates that as z_{ba} increases, the phase boundary shifts to the left similar to the string result (see Fig. 7). Fixing z_1 and z_{we} implies fixing the length of short stickers while increasing z_{ba} corresponds to the increase in the length of long stickers. When one increases z_{ba} , the critical potential depth U_{1C}^{eff} remains the same while the critical potential depth U_{2C}^{eff} decreases.

In addition to unbinding transitions, membranes also undergo lateral phase separation. When $z_1 \neq 0$, the unbinding critical point and the critical point for the lateral phase separation are always detangled. The unbinding transition in this case is second order while the lateral phase transition is first order. In the case of unbinding transition, we can compare membranes and strings either qualitatively or quantitatively as both exhibit continuous

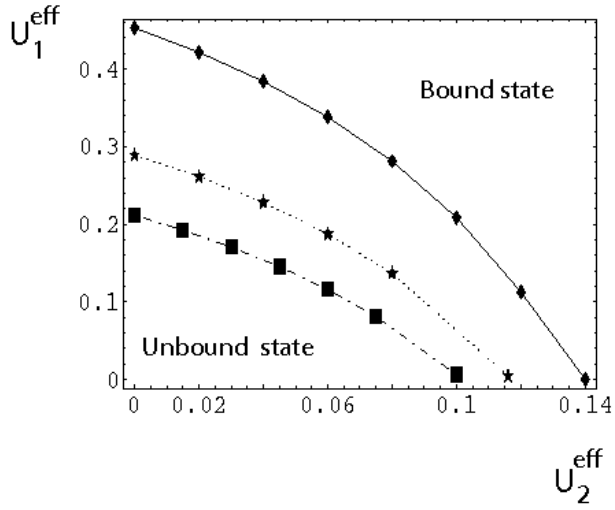


Figure 10: Monte Carlo data for critical potential depths of U_{1C}^{eff} and U_{2C}^{eff} for fixed $z_2 - z_1 = z_{we1} = 0.3$, $z_4 - z_3 = z_{we1} = 0.3$ and $z_3 - z_2 = z_{ba} = 0.2$, $z_1 = 0.1, 0.2$ and 0.3 from right to left. U_{1C}^{eff} and U_{2C}^{eff} decrease as z_1 increases. This result qualitatively agrees with the result displayed in Fig. 6.

unbinding transitions. For strings interacting via double-well potential, the transcendental equation for U_{1C} and U_{2C} is given in Eq. (14). Because membranes and strings have similar scaling properties, we postulate the relation

$$\frac{\sqrt{U_{1C}^{eff}}(z_1\sqrt{U_{1C}^{eff}}k_1 + (z_1 + z_{ba})\sqrt{U_{2C}^{eff}}k_2)}{\sqrt{U_{1C}^{eff}}k_3 + (z_1z_{ba}U_{1C}^{eff} - 1)\sqrt{U_{2C}^{eff}}k_4} = C \quad (16)$$

to hold true for membranes where $k_1 = \cos m_2 \sin m_1$, $k_2 = \cos m_1 \sin m_2$, $k_3 = \cos m_1 \cos m_2$ and $k_4 = \sin m_1 \sin m_2$. Here, $z_{we1} = z_2 - z_1$, $z_{we2} = z_4 - z_1$, $z_{ba} = z_3 - z_2$, $m_1 = z_{we1}\sqrt{U_{1c}^{eff}}$, $m_2 = z_{we2}\sqrt{U_{2c}^{eff}}$. The constant C is obtained from data fitting. We substitute the Monte Carlo data U_{1C}^{eff} , U_{2C}^{eff} , z_{we} , z_{ba} and z_1 in Eq. (16) and evaluate the constant C as a function of z_1 . Similar to the previous section, the constant C saturates to a certain constant C for large values of z_1 . Our analysis shows that at a given value of z_1 , the constant C do not vary significantly. However significant change in C is observed as z_1 increases. The numerical analysis indicates that the constant C saturates to a constant $C = 0.026 \pm 0.003$ as z_1 increases. Using Eq. (16) one can construct a complete phase diagram for unbinding transition of membranes that interact via two species of receptor/ligand bonds. In the limit $z_1 \rightarrow \infty$ or $z_3 \rightarrow \infty$, Eq. (16) converges to Eq. (15). This indicates that membranes interacting with single and double-well potentials should have the same constant C .

4 Summary and conclusions

In this article, we consider strings interacting via a single-well potential. The behavior of the critical potential depth U_c of unbinding from a single-well as a function of model parameters is explored analytically. The critical potential depth U_c decreases when z_1 and z_{we} increase. In the limit $z_{we} \rightarrow \infty$ or $z_{ba} \rightarrow \infty$, $U_c \rightarrow 0$ while $U_c \rightarrow \infty$ in the limit $z_{we} \rightarrow 0$ or $z_{ba} \rightarrow 0$.

For strings interacting with double-well potential, the behavior of the critical points U_{1c} and U_{2c} is studied analytically. The critical potential depths U_{1c} and U_{2c} are functions of z_{we1} , z_{we2} , z_1 and z_{ba} . U_{1c} and U_{2c} decrease as z_{we1} , z_{we2} , z_1 and z_{ba} increase. For fixed z_{ba} , in the limit $z_{we1} = z_{we2} = z_{we} \rightarrow \infty$ or $z_1 \rightarrow \infty$, U_{1c} and U_{2c} go to zero. When $z_{we1} = z_{we2} = z_{we}$ and z_1 are fixed, the critical potential depth $U_{2c} \rightarrow 0$ as $z_{ba} \rightarrow \infty$ while $U_{2c} \rightarrow \infty$ as $z_{ba} \rightarrow 0$.

The Monte Carlo simulation results show that the critical point U_c^{eff} for membranes interacting via single-well potential decreases as z_1 and z_{we} increase similar to the result for strings that interact with single-well potential. On the other hand, the Monte Carlo studying for membranes in an effective double-well potential shows that the critical points U_{1c}^{eff} and U_{2c}^{eff} decrease as the parameters z_1 , z_{we} and z_{ba} increase. We compare the Monte Carlo data of membranes with string analytic result. From scaling property of strings and Monte Carlo simulations, we find a new scaling behavior for membranes interacting via single-well and double-well potentials.

Acknowledgement

It is my pleasure to thank Prof. R. Lipowsky, T. R. Weigl and B. Rozycki for interesting discussions during my stay at Max Planck institute of Colloids and Interfaces Potsdam, Germany. I would like also to thank Hsuan-Yi Chen and Mulugeta Bekele for stimulating discussions.

References

- [1] R. Lipowsky and E. Sackmann, *Structure and Dynamics of Membranes: Generic and Specific Interactions, Vol. 1B of Handbook of Biological Physics* (Elsevier, Amsterdam 1995).
- [2] B. Alberts *et al.*, *Molecular Biology of the Cell*, 3rd edition (Garland, New York, 1994).
- [3] C. R. F. Monks *et al.*, Nature (London), **395**, 82 (1998); G. Grakoui *et al.*, Science, **285**, 221 (1999); D. M. Davis *et al.*, Proc. Natl. Acad. Sci. U.S.A. **96**, 15062 (1999).
- [4] H.-Y. Chen, Phys. Rev. E **67**, 031919 (2003).
- [5] Jia-Yuan Wu and Hsuan-Yi Chen, Phys. Rev. E **73**, 011914 (2006).
- [6] A. Albersdrfer, T. Feder and E. Sackmann, Biophys. J. **73**, 245 (1997).
- [7] T. R. Weigl, R. R. Netz and R. Lipowsky, Phys. Rev. E **62**, R45 (2000).
- [8] T. R. Weigl and R. Lipowsky, Phys. Rev. E **64**, 011903 (2001).

- [9] J. Nardi, T. Feder and E. Sackmann, Europhys. Lett. **37**, 371 (1997).
- [10] H. Strey, M. Peterson and E. Sackmann, Biophys. J. **69**, 478 (1995).
- [11] D. Zuckerman and R. Bruinsma, Phys. Rev. Lett. **74**, 3900 (1995).
- [12] N. J. Burroughs and C. Wlfing, Biophys. J. **83**, 1784 (2002).
- [13] S. Y. Qi, J. T. Groves and A. K. Chakraborty, Proc. Natl. Acad. Sci. U.S.A. **98**, 6548 (2001).
- [14] T. R. Weigl and R. Lipowsky, Biophys. J. **87**, 3665 (2004).
- [15] S. Komura and D. Andelman, Eur. Phys. J. E **3**, 259 (2000).
- [16] R. Bruinsma, A. Behrisch and E. Sackmann, Phys. Rev. E **61**, 4253 (2000).
- [17] M. Asfaw, B. Rozycki, R. Lipowsky and T. R. Weigl, Europhys. Lett. **76**, 703 (2006).
- [18] R. Lipowsky and B. Zielinska, Phys. Rev. Lett. **62**, 1572 (1989).
- [19] R. Lipowsky and S. Leibler, Phys. Rev. Lett. **56**, 2541 (1986).
- [20] R. Lipowsky, Europhys. Lett. **7**, 703 (1991).
- [21] F. Wiegler, *Introduction to Path-Integral Methods in Physics and Polymer Science*, (World Scientific, Philadelphia, 1986).
- [22] T. Franke, R. Lipowsky and W. Helfrich, Europhys. Lett. **76**, 339 (2006).
- [23] R. Lipowsky, Europhys. Lett. **7**, 255 (1988).
- [24] B. Rozycki and M. Napiorkowski, Europhys. Lett. **66**, 35 (2004).
- [25] L. S. Schulman, *Techniques and Applications of Path Integration*, (Dover, 2005).
- [26] David J. Griffiths, *Introduction to Quantum Mechanics* (Prentice Hall, 2004).
- [27] K. Binder and D. W. Heermann, *Monte Carlo Simulation in Statistical Physics* (Springer, Berlin 1992).